Journal of Molecular Structure 987 (2011) 206–213

Contents lists available at ScienceDirect

Journal of Molecular Structure

journal homepage: www.elsevier.com/locate/molstruc

Synthesis, characterization and structural aspects of new haptens for PAHs

Yi Li [a], Mingming Yang [b], Yuanyuan Liu [b], Rongqing Wei [a], Xiaoning Liu [a,*], Fangshi Li [b,*]

[a] College of Biotechnology and Pharmaceutical Engineering, Nanjing University of Technology, Nanjing 210009, PR China
[b] College of Science, Nanjing University of Technology, Nanjing 210009, PR China

ARTICLE INFO

Article history:
Received 2 November 2010
Received in revised form 13 December 2010
Accepted 13 December 2010
Available online 21 December 2010

Keywords:
Hapten of PAHs
4-(Naphthalen-2-yl)-4-oxobutanoic acid
4-(Anthracen-1-yl)-4-oxobutanoic acid
Crystal structure
Hartree–Fock calculation

ABSTRACT

Two new haptens for PAHs, 4-(naphthalen-2-yl)-4-oxobutanoic acid (**I**) and 4-(anthracen-1-yl)-4-oxobutanoic acid (**II**), were synthesized and confirmed by elemental analysis, IR, and ^{1}H NMR. Single crystal X-ray structure showed that compound **I** crystallizes in the triclinic crystal system (space group = P-1). A classic hydrogen bonded dimer is formed by the carboxylic acid group from two molecules. The $\mathbf{R}_2^2$ (**8**) graph-set motif links the molecules into pairs around inversion centers in the unit cell. The O–H···O hydrogen-bonded interactions involving these pairs are very strong and stabilize molecular packing of these dimers into a unique assembly. Compound **II** crystallizes in the Monoclinic crystal system (space group = P21/c). Similarly to compound **I**, a classic hydrogen bonded dimer is formed by the carboxylic acid group from two molecules. The $\mathbf{R}_2^2$ (**8**) graph-set motif links the molecules into pairs around inversion centers in the unit cell. Besides, an intramolecular hydrogen bonding causes the formation of a planar six-membered ring, which is also coplanar with the adjacent anthracene ring. The geometries of the corresponding parts of the haptens are almost the same as those of naphthalene and anthracene. Ab initio Hartree–Fock computational calculation provided the supports that the size, shape (geometry) and electronic properties at the corresponding parts of the haptens did not change significantly, compared to those of naphthalene and anthracene. The haptens were coupled with bovine serum albumin (BSA) to make antigents. The coupling ratio of **I-BSA** was **1:20**, and **II-BSA 1:37**, respectively. These results showed that the new haptens could be used to induce specific antibodies for PAHs.

© 2010 Elsevier B.V. All rights reserved.

1. Introduction

Polycyclic aromatic hydrocarbons (PAHs) are a large group of organic compounds containing two or more fused aromatic rings constituted of carbon and hydrogen atoms. PAHs have received considerable attention because of their rich chemistry [1–5], physical properties [6], technological and industrial applications [1], aromaticity [7–15], and role as a major class of environmental pollutants and carcinogens [16–18].

Conventional analytical methods for PAHs, such as gas chromatography (GC) and high-performance liquid chromatography (HPLC), are time-consuming and cumbersome [19–21]. Immunochemical methods, such as enzyme-linked immunosorbent assays (ELISAs) and immunosensors, are fast, selective, and inexpensive analytical methods that complement traditional chromatographic analytical procedures in the environmental analysis of PAHs [22–27].

Immunochemical methods are based on the specific interaction of antibodies with antigens. PAHs are low-molecular-mass molecules that are unable to induce an immune response. Therefore, the target molecule is derivatized into a hapten, by introducing a functional group, in order to link it to a carrier protein, for example, bovine serum albumin (BSA). The immunoconjugate thus formed is immunogenic and a mammal can be immunized to produce specific antibodies to the antigen. The key step in developing an immunoassay for PAHs is the design and preparation of optimum haptens for immunogens and competitors. The performance of the antibody in immunoassays is greatly affected by the property of the hapten.

There have been some haptens for PAHs reported [26,28,24], however, the antibody specificity resulting from the newly designed hapten is often unpredictable, and this knowledge comes only after time-consuming and laborious animal experiments.

It would be more attractive to be able to predict the specificity of the antibodies obtained with a given hapten. As antigen–antibody recognition is based on the steric criteria and the interactions resulting from the electronic properties of the molecules, molecular modeling may be helpful as it allows the determination of volumes and charges of the compounds [29].

To have a better understanding of such hapten molecules from the molecular and sub-molecular level, we report here the synthesis of two novel haptens for PAHs (Fig. 1, compounds **I** and **II**). The

* Corresponding authors. Tel./fax: +86 25 83587347 (X. Liu), tel./fax: +86 25 83587450 (F. Li).
E-mail addresses: xiaoningliu@163.com (X. Liu), fangshi.li@njut.edu.cn (F. Li).

0022-2860/$ - see front matter © 2010 Elsevier B.V. All rights reserved.
doi:10.1016/j.molstruc.2010.12.023

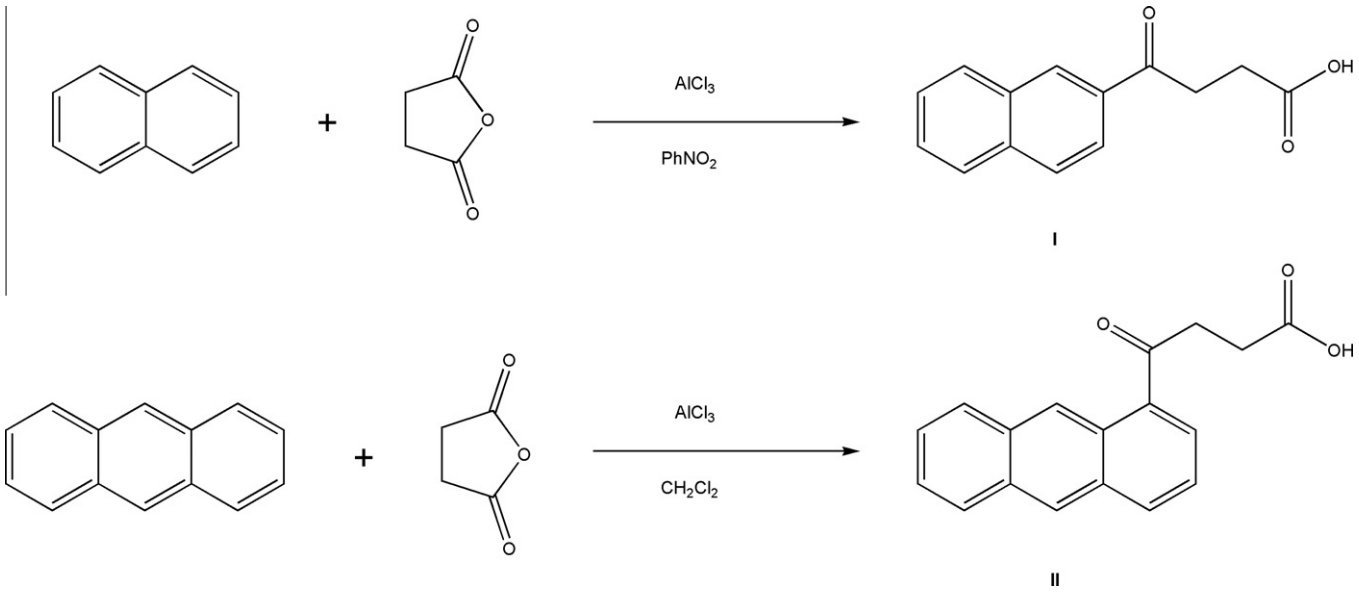

Fig. 1. Scheme of the synthesis of compounds **I** and **II**.

crystal structure and the isolated state conformation of the haptens were studied by X-ray crystallography and ab initio calculation. And the electronic structures of the haptens and the conjugates were discussed.

2. Experimental

2.1. Materials and instruments

All chemicals were reagent grade and were used without further purification.

^{1}H NMR spectra were recorded on a Bruker AV-500 spectrometer at 500 MHz or a Bruker AV-300 spectrometer at 300 MHz using $CDCl_3$ or DMSO-d6 as the solvent, with tetramethylsilane as the internal standard. Chemical shifts (δ) are given in parts per million (ppm), and coupling constants (J) are given in Hertz (Hz). IR spectra were recorded in KBr disk using a Nicolet 380 FT-IR spectrophotometer and only diagnostic absorbances (λ_{max}) are reported. Elemental analyses were performed with a Flash EA-1112 elemental analyzer. Melting points were measured on an X-4 microscope electrothermal apparatus and were uncorrected. X-ray crystallographic analyses were performed on a Nonius CAD4 single-crystal diffractometer using graphite-monochromated Mo Kα radiation (λ = 0.71073) Å.

2.2. Synthesis of 4-(naphthalen-2-yl)-4-oxobutanoic acid (*I*)

Hapten (**I**) was synthesized according to the method reported in the literature [30] with some modification. A suspension of naphthalene (3.84 g, 0.03 mol) and succinic anhydride (3.0 g, 0.03 mol) in $PhNO_2$ (60 mL) was cooled in an ice bath, and $AlC1_3$ (8.5 g, 0.065 mol) was added in four portions over 20 min with vigorous mechanical stirring. The mixture was stirred at 0–5 °C for 10 h, and then at 25 °C for 24 h. Ice and dilute HCl were added with stirring. The mixture was decanted. The brown solid was separated and washed thoroughly with H_2O and Hexane. The solid was triturated with a small amount of benzene and air-dried. m.p. 157–159 °C; Yield: 2.8 g, 41%. *Anal. calcd.* for $C_{14}H_{12}O_3$: C 73.67, H 5.30; found C 73.52, H 5.32. IR (KBr, ν, cm^{-1}): 3059, 2931, 1714, 1680, 1624, 1433, 1403, 1367, 1254, 1230, 1170, 933, 812; ^{1}H NMR (300 MHz, $CDCl_3$) δ 8.51 (s, 1H, Ar–H), 8.06–7.54 (m, 6H, Ar–H), 3.48 (t, J = 6.7 Hz, 2H, CH_2), 2.89 (t, J = 6.7 Hz, 2H, CH_2).

2.3. Synthesis of 4-(anthracen-1-yl)-4-oxobutanoic acid (*II*)

Hapten (**II**) was synthesized according to the method reported in the literature [31] with some modification. A suspension of anthracene (7.14 g, 0. 04 mol) and succinic anhydride (4.0 g, 0.04 mol) in CH_2C1_2 (100 mL) was cooled in an ice bath, and $AlC1_3$ (5.5 g, 0.041 mol) was added in four portions over 20 min with vigorous mechanical stirring. The deep-red mixture was stirred at 0–5 °C for another 60 min and stored in the refrigerator overnight. Ice and dilute HCl were added with stirring to decompose the complex. The mixture was digested on a boiling water bath for 2 h to evaporate the organic solvent. The mixture was cooled and decanted. The solid was separated and washed thoroughly with H_2O. The solid was digested with dilute K_2CO_3 solution on a boiling water bath for 30 min. The remaining solid was collected by filtration. To the filtrate, EtOAc (100 mL) was added, followed by the dropwise addition of concentrated HCl with stirring. The layers were separated and the aqueous layer was extracted with EtOAc. The combined organic extracts were dried (Na_2SO_4) and evaporated under reduced pressure. The oily residue was treated with a small amount of benzene. The yellow precipitate was filtered, air-dried, and recrystallized from EtOAc. m.p. 177–179 °C; yield: 3.1 g, 55%. *Anal. calcd.* for $C_{18}H_{14}O_3$: C 77.68, H 5.07; found: C 77.56, H 5.10. IR (KBr, ν, cm^{-1}): 3042, 2921, 1710, 1671, 1615, 1537, 1408, 1349, 1254, 1197, 1169, 1081, 958, 903, 877, 732. ^{1}H NMR (500 MHz, DMSO-d6) δ 12.20 (s, 1H, OH), 9.22 (s, 1H, Ar–H), 8.68 (s, 1H, Ar–H), 8.33–8.08 (m, 4H, Ar–H), 7.62–7.56 (m, 3H, Ar–H), 3.40 (t, J = 6.5 Hz, 2H, CH_2), 2.72 (t, J = 6.5 Hz, 2H, CH_2).

2.4. Preparation of Hapten-protein conjugates

The hapten-protein conjugates were prepared by the slightly modified NHS ester method [32]. The coupling ratio of **I-BSA** was 1:20, and **II-BSA** 1:37, respectively.

2.5. X-ray structure determination of the haptens

Colorless crystals of **I** suitable for X-ray analysis were grown from concentrated solution of methanol, and yellow crystals of **II** from acetonitrile.

A crystal was put on a glass fiber. The diffraction data were collected on a Nonius CAD4 single-crystal diffractometer equipped with a graphite-monochromated Mo Kα radiation (λ = 0.71073 Å) by using a $\omega/2\theta$ scan mode at 298 K. The crystal structure was solved by the direct method and refined by the full-matrix least-squares procedure on F^2 using SHELXL-97 program [33]. Positions of hydrogen atoms were located by geometrical calculation (x, y, z and Uiso fixed to 1.2 times Uiso of the atom they are bound to).

Crystal and experimental data for **I** and **II** are listed in Table 1. The atomic coordinates of non-hydrogen atoms and their thermal parameters of **I** and **II** are listed in Tables 2 and 3. The bond lengths and bond angles are listed in Table 4. The molecular structures of **I** and **II** are shown in Figs. 2 and 4, respectively.

Table 1
X-ray crystal data and structure refinement of **I** and **II**.

Chemical formula	**I**	**II**
Formula weight	$C_{14}H_{12}O_3$	$C_{18}H_{14}O_3$
CCDC number	759778	798276
Temperature (K)	293(2)	293(2)
Wavelength (Å)	0.71073	0.71073
Crystal system, Space group	Triclinic, P-1 (No. 2)	Monoclinic, P21/c (No. 14)
a (Å)	5.6250(11)	18.021(4)
b (Å)	7.6220(15)	5.2290(10)
c (Å)	13.537(3)	14.788(3)
α (°)	99.36(3)	90.00
β (°)	97.39(3)	90.51(3)
γ (°)	99.14(3)	90.00
V (Å^3), Z	558.23(19), 2	1393.4(5), 4
Density (calc.) (g cm^{-3})	1.358	1.327
Abs. coeff. (mm^{-1})	0.095	0.090
F(0 0 0)	240	584
θ Ranges (data collection)	1.54–25.27	1.13–25.29
Index ranges	$0 \leqslant h \leqslant 6$ $-9 \leqslant k \leqslant 9$ $-16 \leqslant l \leqslant 16$	$-21 \leqslant h \leqslant 0$ $0 \leqslant k \leqslant 6$ $-17 \leqslant l \leqslant 17$
Reflections collected	2248	2622
R_{int}	0.013	0.091
Independent reflections	2026	2538
Refinement method on F^2	Full-matrix least-squares	Full-matrix least-squares
Goodness-of-fit on F^2	1.004	1.002
Final R indices [$I > 2\sigma(I)$]	0.0488	0.0674
R indices (all data)	0.0632	0.1641
Residual (e Å^{-3})	0.144/−0.272	0.145/−0.133

Table 2
Atomic coordinates of non-hydrogen atoms (**I**) and their thermal parameters.

Atom	x	y	z	U (eq)
O1	0.6995(3)	0.8657(2)	1.46691(9)	0.0765(5)
O2	0.9663(2)	0.9652(2)	1.37329(9)	0.0642(5)
O3	0.2354(2)	0.6741(2)	1.12317(9)	0.0701(5)
C1	0.7661(3)	0.8856(2)	1.38016(12)	0.0470(5)
C2	0.5705(3)	0.8013(2)	1.29244(12)	0.0473(5)
C3	0.6424(3)	0.8189(2)	1.19024(12)	0.0435(4)
C4	0.4342(3)	0.7365(2)	1.10492(13)	0.0428(4)
C5	0.4727(3)	0.7352(2)	0.99783(12)	0.0384(4)
C6	0.2826(3)	0.6536(2)	0.92175(12)	0.0395(4)
C7	0.3038(3)	0.6510(2)	0.81878(12)	0.0391(4)
C8	0.1079(3)	0.5685(3)	0.73941(13)	0.0504(5)
C9	0.1326(4)	0.5714(3)	0.64160(14)	0.0600(5)
C10	0.3532(4)	0.6558(3)	0.61678(14)	0.0600(6)
C11	0.5450(3)	0.7353(2)	0.69075(13)	0.0512(5)
C12	0.5261(3)	0.7353(2)	0.79394(12)	0.0396(4)
C13	0.7203(3)	0.8173(2)	0.87373(13)	0.0469(5)
C14	0.6957(3)	0.8166(2)	0.97201(13)	0.0465(5)

2.6. Quantum chemical calculations

The first task for the computational work was to determine the optimized geometry of the compounds **I** and **II**. The spatial coordinate positions of the compounds **I** and **II**, as obtained from the X-ray structural analysis, were used as the initial coordinates for their theoretical calculations. The quantum mechanical calculations were carried out using the Gaussian 03 program using the Hartree–Fock (HF) method with a 6-31G (d) basis set level [34,35]. The geometrical, electronic, and energy parameters were extracted from the Gaussian files based on the optimized structures.

3. Results and discussion

3.1. Hapten design

For any kind of immunochemical method, the specific antibody is the key reagent. To produce antibody against a small molecule like a PAH, the latter must be conjugated with a carrier, usually some protein such as albumin [36,37]. Unfortunately, PAHs have no functional group for direct conjugation with proteins. Therefore, a derivative (hapten) of PAH must be synthesized. According the criteria of structure design for haptens [38–40], that the hapten should be a near perfect mimic of the target structure in size, shape (geometry), and electronic properties, we designed two new haptens for PAHs (Fig. 1). Hapten **I** has a carboxyl group with four length of spacer arm at 2-position of naphthalene, and **II** at 1-position of anthracene.

3.2. Single crystal X-ray crystallography of the haptens

Single crystal X-ray diffraction study has shown that compound **I** crystallizes in the Triclinic crystal system (space group = P-1). A packing diagram of **I** in the unit cell is shown in Fig. 3. A classic hydrogen bonded dimer is formed by the carboxylic acid group from two molecules (Table 5). The $\mathbf{R}_2^2$ (**8**) graph-set motif [41] links the molecules into pairs around inversion centers in the unit cell. The O–H···O hydrogen-bonded interactions involving these pairs are very strong and stabilize molecular packing of these dimers

Table 3
Atomic coordinates of non-hydrogen atoms (**II**) and their thermal parameters.

Atom	x	y	z	U (eq)
C1	0.26224(17)	0.8180(7)	0.2685(2)	0.0525(9)
O1	0.19395(15)	0.4585(6)	0.13925(16)	0.0970(10)
C2	0.29759(18)	0.8428(7)	0.1850(2)	0.0613(10)
O2	0.01361(15)	0.4799(6)	0.11187(18)	0.0986(10)
C3	0.35175(18)	1.0295(7)	0.1704(2)	0.0595(10)
O3	0.05722(14)	0.2233(5)	0.00616(19)	0.0943(10)
C4	0.3879(2)	1.0498(8)	0.0856(2)	0.0780(12)
C5	0.4410(2)	1.2291(9)	0.0713(3)	0.0899(14)
C6	0.4607(2)	1.3985(9)	0.1431(4)	0.0898(14)
C7	0.4295(2)	1.3825(8)	0.2239(3)	0.0811(12)
C8	0.37356(19)	1.1960(7)	0.2422(3)	0.0606(10)
C9	0.3386(2)	1.1699(8)	0.3248(2)	0.0680(11)
C10	0.28497(19)	0.9862(7)	0.3408(2)	0.0572(10)
C11	0.2506(2)	0.9636(8)	0.4260(2)	0.0778(12)
C12	0.1975(2)	0.7865(9)	0.4420(2)	0.0837(13)
C13	0.1747(2)	0.6244(7)	0.3722(2)	0.0660(11)
C14	0.20430(18)	0.6312(6)	0.2870(2)	0.0504(9)
C15	0.17310(17)	0.4597(7)	0.2176(2)	0.0572(10)
C16	0.11276(18)	0.2713(7)	0.2411(2)	0.0637(10)
C17	0.08697(19)	0.1240(8)	0.1594(3)	0.0763(12)
C18	0.0501(2)	0.2924(8)	0.0904(3)	0.0717(11)

Table 4
Theoretical and X-ray crystallography data of **I** and **II**.

I			**II**		
Parameters	X-ray	Calculated	Parameters	X-ray	Calculated
O1–C1	1.302(2)	1.3299	C1–C2	1.400(4)	1.3907
O2–C1	1.214(2)	1.1891	C1–C10	1.441(4)	1.4299
O3–C4	1.216(2)	1.197	C1–C14	1.458(4)	1.4505
C1–C2	1.492(2)	1.5055	O1–C15	1.221(3)	1.1959
C2–C3	1.511(2)	1.5216	C2–C3	1.399(4)	1.3914
C3–C4	1.511(2)	1.5176	O2–C18	1.223(4)	1.1867
C4–C5	1.492(2)	1.4997	C3–C4	1.423(4)	1.4354
C5–C6	1.374(2)	1.3654	C3–C8	1.426(4)	1.4209
C5–C14	1.420(2)	1.4218	O3–C18	1.305(4)	1.3317
C6–C7	1.412(2)	1.4149	C4–C5	1.356(5)	1.348
C7–C12	1.419(2)	1.4091	C5–C6	1.425(5)	1.4322
C7–C8	1.421(2)	1.4216	C6–C7	1.328(5)	1.3478
C8–C9	1.352(3)	1.3573	C7–C8	1.430(5)	1.435
C9–C10	1.411(3)	1.4176	C8–C9	1.385(5)	1.3883
C10–C11	1.360(3)	1.3582	C9–C10	1.384(5)	1.3885
C11–C12	1.414(2)	1.4202	C10–C11	1.414(4)	1.4344
C12–C13	1.418(2)	1.4194	C11–C12	1.354(5)	1.3453
C13–C14	1.356(2)	1.3575	C12–C13	1.396(5)	1.4271
			C13–C14	1.372(4)	1.3546
O2–C1–O1	122.66(15)	122.2805	C14–C15	1.472(4)	1.5058
O2–C1–C2	124.72(16)	125.9762	C15–C16	1.510(4)	1.5252
O1–C1–C2	112.62(15)	111.7434	C16–C17	1.503(4)	1.5273
C1–C2–C3	114.19(15)	112.0937	C17–C18	1.499(5)	1.5102
C4–C3–C2	111.61(14)	112.1655			
O3–C4–C5	120.04(15)	120.7656	C2–C1–C10	118.0(3)	117.8507
O3–C4–C3	120.41(15)	120.6854	C2–C1–C14	124.1(3)	124.1966
C5–C4–C3	119.54(14)	118.549	C10–C1–C14	117.9(3)	117.9041
C6–C5–C14	119.17(15)	119.2261	C3–C2–C1	121.7(4)	122.1844
C6–C5–C4	118.20(15)	118.0797	C2–C3–C4	121.0(4)	121.8723
C14–C5–C4	122.62(15)	122.6942	C2–C3–C8	119.9(3)	119.5772
C5–C6–C7	121.34(15)	121.3972	C4–C3–C8	119.1(4)	118.5502
C6–C7–C12	119.00(15)	119.0342	C5–C4–C3	121.2(4)	120.8095
C6–C7–C8	121.90(15)	121.7855	C4–C5–C6	119.0(4)	120.5773
C12–C7–C8	119.10(15)	119.1803	C7–C6–C5	121.8(4)	120.4241
C9–C8–C7	120.42(17)	120.6154	C6–C7–C8	121.2(4)	120.7333
C8–C9–C10	120.56(18)	120.1566	C9–C8–C3	118.1(4)	118.6163
C11–C10–C9	120.61(17)	120.5423	C9–C8–C7	124.1(4)	122.4741
C10–C11–C12	120.51(17)	120.5537	C3–C8–C7	117.7(4)	118.9043
C11–C12–C13	122.59(15)	122.2415	C10–C9–C8	122.9(4)	121.8089
C11–C12–C7	118.80(15)	118.9517	C9–C10–C11	121.5(4)	120.5586
C13–C12–C7	118.62(15)	118.8068	C9–C10–C1	119.4(3)	119.9184
C14–C13–C12	121.19(15)	120.9283	C11–C10–C1	119.1(4)	119.5102
C13–C14–C5	120.67(15)	120.6074	C12–C11–C10	121.9(4)	120.8871
			C11–C12–C13	119.4(4)	119.9011
			C14–C13–C12	123.3(4)	121.9999
			C13–C14–C1	118.4(3)	119.7144
			C13–C14–C15	118.4(3)	114.866
			C1–C14–C15	123.1(3)	125.3693
			O1–C15–C14	123.1(3)	120.0166
			O1–C15–C16	116.3(3)	119.2785
			C14–C15–C16	120.6(3)	120.5029
			C17–C16–C15	111.6(3)	111.817
			C18–C17–C16	112.2(3)	116.0185
			O2–C18–O3	121.8(4)	122.2231
			O2–C18–C17	122.0(4)	124.1248
			O3–C18–C17	116.1(4)	113.6265

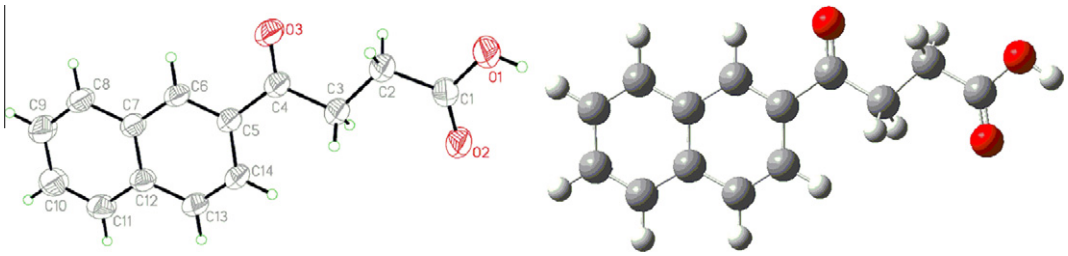

Fig. 2. (Left): X-ray structure with atoms numbering of **I**. Ellipsoids are drawn at 50% probability. (Right): The theoretical optimized geometric structure of **I**.

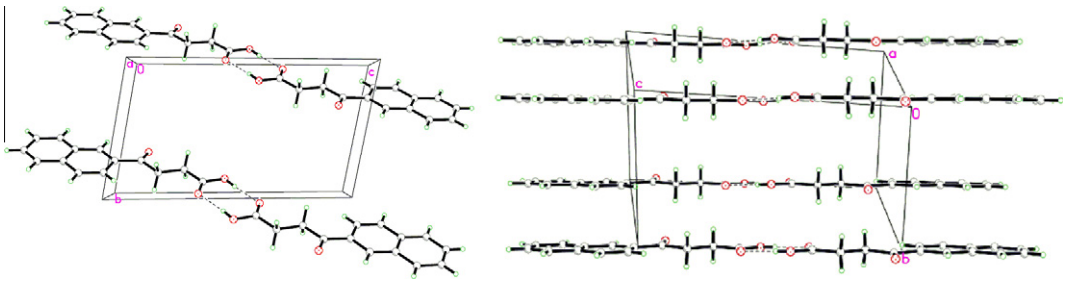

Fig. 3. Packing diagram of **I** in the unit cell. Hydrogen bonds are shown as dashed lines.

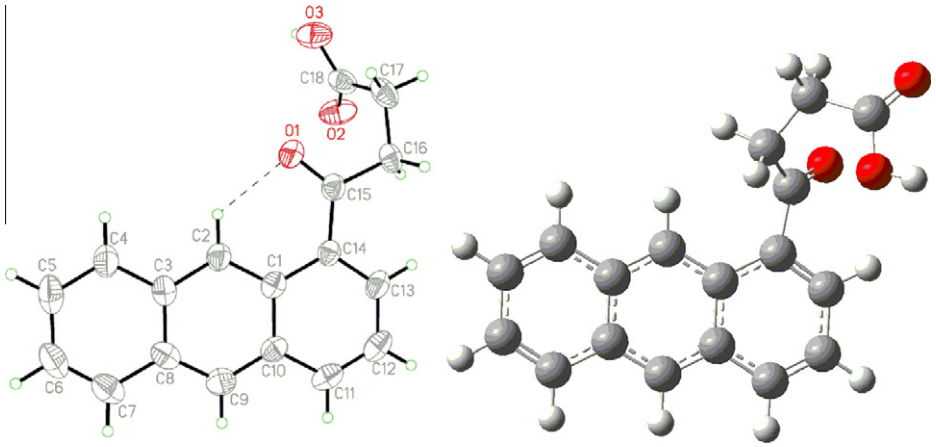

Fig. 4. (Left): X-ray structure with atoms numbering of **II**. Ellipsoids are drawn at 50% probability. (Right): The theoretical optimized geometric structure of **II**.

Table 5
Hydrogen bonding parameters (Å, °) of **I**.

D–H···A	*d*(D–H)	*d*(H···A)	*d*(D···A)	<D–H···A
O1–H1A–O2 #1	0.8200	1.8600	2.6743(19)	174.00

Symmetry transformations used to generate equivalent atoms #1 $2-x, 2-y, 3-z$.

Table 6
Hydrogen bonding parameters (Å, °) of **II**.

D–H···A	*d*(D–H)	*d*(H···A)	*d*(D···A)	<D–H···A
O3–H3A–O2 #1	0.8200	1.8400	2.654(4)	173.00
C2–H2A–O1	0.9300	2.1700	2.822(5)	126.00

Symmetry transformations used to generate equivalent atoms: #1 $-x, 1-y, -z$.

into a unique assembly. The naphthalene ring parts are plane (the dihedral angle of C9–C8–C7–C6 is 1.27°) and form parallel layers with a distance of 2.870 Å between the dimers. The dihedral angle of the naphthalene ring and the $\mathbf{R}_2^2$ (**8**) graph-set motif is 3.52°.

Compound **II** crystallizes in the Monoclinic crystal system (space group = P21/c). A packing diagram of **II** in the unit cell is shown in Fig. 5. Similarly to compound **I**, a classic hydrogen bonded dimer is formed by the carboxylic acid group from two molecules (Table 6). The $\mathbf{R}_2^2$ (**8**) graph-set motif links the molecules into pairs around inversion centers in the unit cell. Besides, The intramolecular C2–H···O1 hydrogen bonding causes the formation of a planar six-membered ring, which is also coplanar with the adjacent anthracene ring (Fig. 5 and Table 6). The anthracene ring parts are plane (the dihedral angle of C5–C4–C3–C2 is 0.62° and C3–C2–C1–C14 is 1.45°) and form parallel layers with a distance of 2.484 Å between the dimers. The dihedral angle of the anthracene ring and the $\mathbf{R}_2^2$ (**8**) graph-set motif is 80.08°.

According to the X-ray data in Table 4, the bond lengths and angles of the corresponding parts of **I** and **II** are almost same with those of naphthalene and anthracene [12]. The biggest difference between **I** and naphthalene is 0.0099 Å at (C_7–C_{12}), while between **II** and anthracene is 0.0311 Å at (C_{12}–C_{13}), respectively.

3.3. Quantum chemical calculations

3.3.1. Molecular geometry of the haptens

For comparison with the X-ray study, the optimized structures of **I** and **II** by HF calculations are shown in Figs. 2 and 4, respectively.

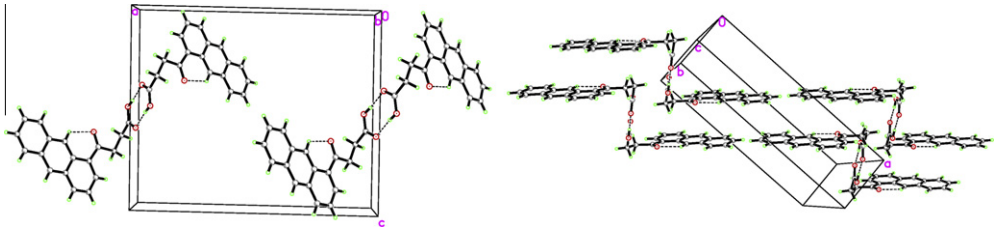

Fig. 5. Packing diagram of **II** in the unit cell. Hydrogen bonds are shown as dashed.

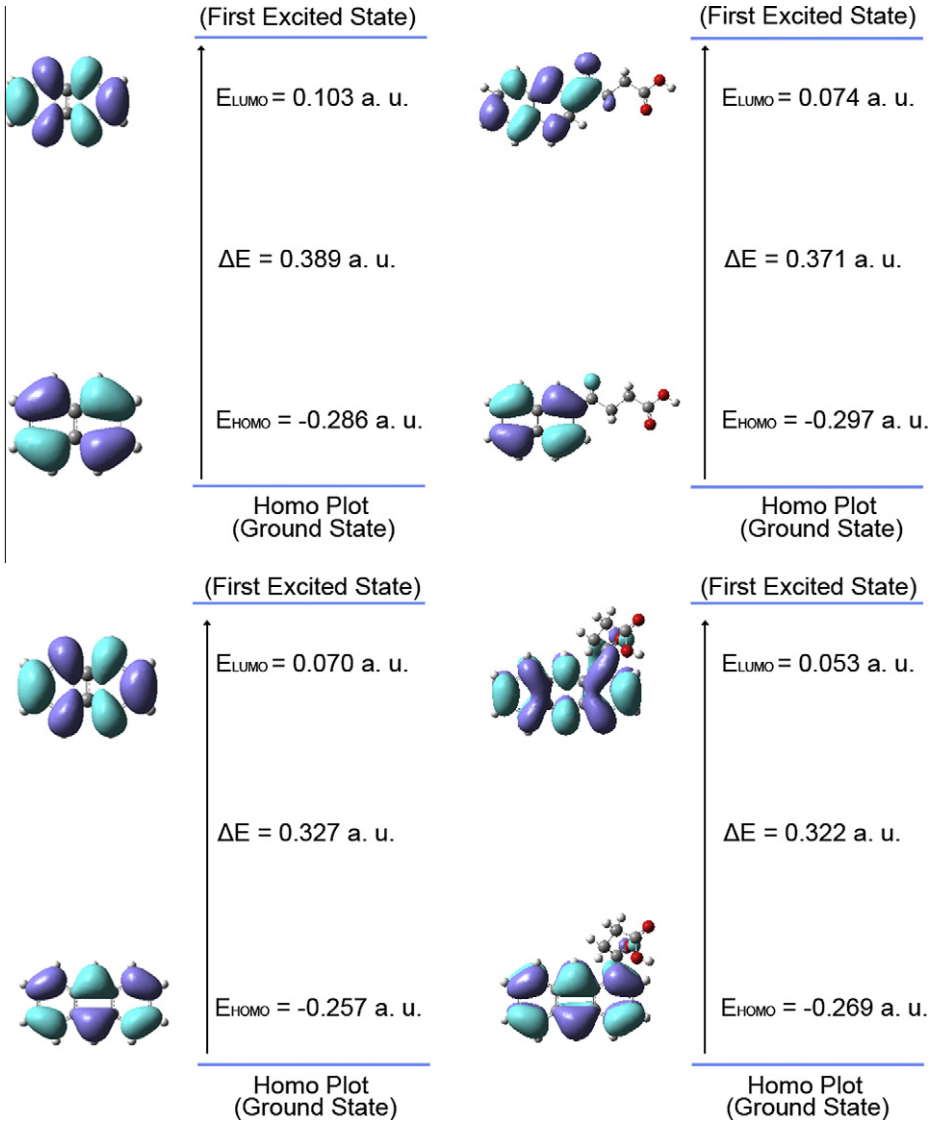

Fig. 6. The frontier molecular orbitals (HOMO and LUMO) for **I** and **II** by using HF.

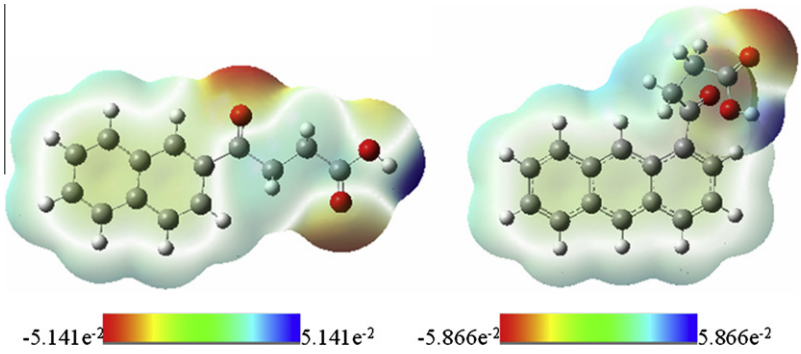

Fig. 7. The electrostatic potential isosurfaces of **I** and **II**. The blue areas indicate positive potential and the red areas indicate negative potential.

It is interesting that the orientation of the O1 atom in the theoretically computed molecule and in the molecule calculated from diffraction data is absolutely different (Fig. 4). The reason perhaps is that the calculation was based on an isolated gaseous molecule, while the X-ray diffraction on solid-state molecules. Crystal particles present periodically ordered in the micro space. It is the order that fix the orientation of the O1 atom in crystal state.

The optimized structure parameters are also listed in Table 4. Because of the hydrogen bonds (Figs. 3 and 5, Tables 5 and 6), the theoretical values of the bond lengths and angles related to

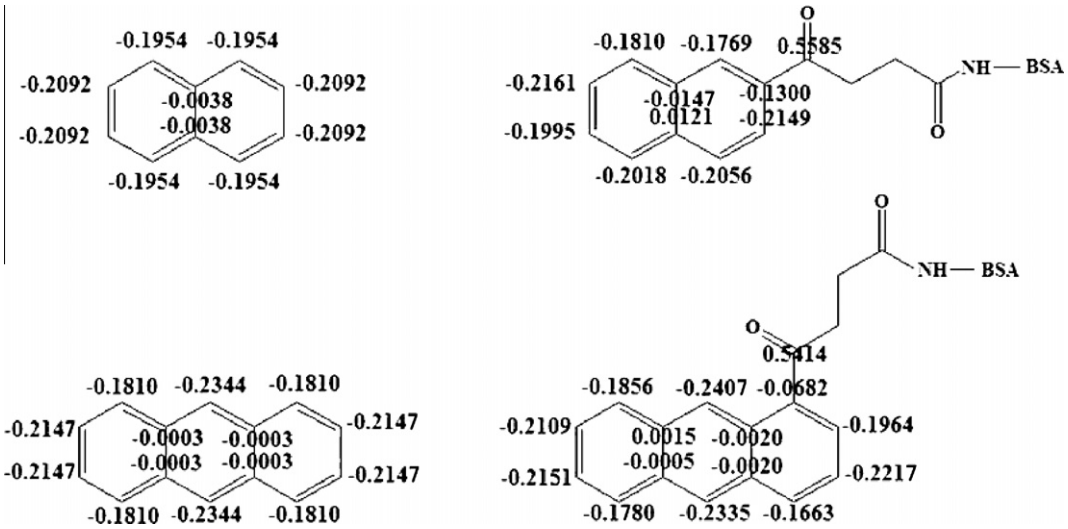

Fig. 8. The charge distribution of **I-BSA** and **II-BSA**.

the carboxyl groups are some different from their crystal data. Whereas other parameters computed are almost same with the values obtained from X-ray crystallographic data.

3.3.2. Frontier molecular orbital and energies of the haptens

The frontier-orbital energies of a compound can play an important role in biological activity [42]. E_{HOMO} is a rough measure of the electron-donating ability of a compound and, normally, increasing its value can increase the biological activity, while the E_{LUMO} acts in reverse. It is clear from the graphical representation of the HOMO and LUMO for **I** and **II** (Fig. 6), that the electron cloud of HOMO is mainly focused on the naphthalene and anthracene rings. These parts were most likely the important portions of the epitopes for antibody recognition.

3.3.3. Electrostatic potential isosurface map of the haptens

From the electrostatic potential isosurface map of a compound, we can get which region is electron rich region, which is the lack e-region, so we can know which atoms susceptible to nucleophile attack, which attacked by electrophilic reagents.

Fig. 7 is the electrostatic potential isosurface maps of **I** and **II**. The blue areas indicate positive potential and the red areas indicate negative potential. For the corresponding parts of naphthalene and anthracen, the positive electrostatic potential is more evenly distributed at the edge of the rings. The negative electrostatic potential is distributed in both sides of the ring plane. Compared to those of naphthalene and anthracen [43], the electrostatic potential isosurface of the corresponding parts of **I** and **II** do not change significantly.

3.3.4. Charge distribution of the conjugates

The immunoconjugate region determines the priority of the recognition sites of the antibodies. The more the similarity between the corresponding region of a compound and the specific region of an immunoconjugate, the higher the affinity of the resulting antibodies for this analyte.

The charge distributions of naphthalene, anthracen, and the conjugates are shown in Fig. 8 for comparison. The biggest change of the charge distribution at the corresponding parts of **I-BSA** and **II-BSA** is at the carbon atom connected to the carbonyl group. The changes are from (−0.2092) e to (−0.1300) e for **I-BSA**, and from (−0.1810) to (−0.0682) for **II-BSA**, respectively. The changes are not significant.

4. Conclusion

Two new haptens for PAHs were synthesized. Hapten **I** has a carboxyl group with four length of spacer arm at 2-position of naphthalene, and **II** at 1-position of anthracene. Single crystal X-ray structure showed that a classic O–H···O hydrogen bonded dimmer is formed by the carboxylic acid group for both of the haptens. The geometries of the corresponding parts of the haptens are almost the same as naphthalene and anthracene. The HF computational calculations provided the supports that the size, shape (geometry) and electronic properties at the corresponding parts of the haptens did not change significantly, compared to naphthalene and anthracene. These results showed that the new haptens could be used to induce antibodies for PAHs.

Supplementary material

Crystallographic data for the structural analysis of the synthesized compounds have been deposited at the Cambridge Crystallographic Data Center, 12 Union Road, Cambridge, CB2 1EZ, UK, and are available free of charge from the Director on request quoting the deposition number CCDC 759778 and 798276 (fax: C44 1223 336033, e-mail: deposit@ccdc.cam.ac.uk).

Acknowledgement

This work was supported by the National High-tech R&D Program of China (No. 2007AA02Z200 and 2007AA06A402).

References

[1] R.G. Harvey, Polycyclic Aromatic Hydrocarbons, John Wiley, New York, 1997.
[2] P. Garrigues, M. Lamotte, Polycyclic Aromatic Compounds: Synthesis, Properties, Analytical Measurements, Occurrence and Biological Effects, Gordon and Breach Science Publishers, Amsterdam, 1993.
[3] J.R. Dias, Handbook of Polycyclic Hydrocarbons: Part A, Benzenoid Hydrocarbons (Physical Sciences Data, No. 30), Elsevier, New York, 1987.
[4] J.C. Fetzer, Large (C ⩾ 24) Polycyclic Aromatic Hydrocarbons: Chemistry and Analysis, John Wiley, New York, 2000.
[5] M.L. Lee, M.V. Novotny, K.D. Bartle, Analytical Chemistry of Polycyclic Aromatic Compounds, Academic Press, New York, 1981.
[6] R.A. Hites, W.J. Simonsick Jr., Calculated Molecular Properties of Polycyclic Aromatic Hydrocarbons, Elsevier, New York, 1987.
[7] P.V.R. Schleyer, Chem. Rev. 101 (2001) 1115.
[8] G. Portella, J. Poater, J.M. Bofill, P. Alemany, M. Sola, J. Org. Chem. 70 (2005) 2509.
[9] J. Poater, X. Fradera, M. Duran, M. Sola, Chem. Eur. J. 9 (2003) 400.

[10] K.B. Wiberg, J. Org. Chem. 62 (1997) 5720.
[11] S.T. Howard, T.M. Krygowski, Can. J. Chem. 75 (1997) 1174.
[12] C.H. Suresh, S.R. Gadre, J. Org. Chem. 64 (1999) 2505.
[13] P.J. Garratt, Aromaticity, Wiley, New York, 1986.
[14] E. Clar, The Aromatic Sextet, John Wiley and Sons Ltd., London, 1972.
[15] G.M. Badger, Aromatic Character and Aromaticity, Cambridge University Press, Cambridge, 1969.
[16] A.H. Neilson, PAHs and Related Compounds: Biology, Springer, New York, 1998.
[17] A. Luch, The Carcinogenic Effects of Polycyclic Aromatic Hydrocarbons, Imperial College Press, London, 2005.
[18] D.M. Jerina, H. Yagi, R.E. Lehr, D.R. Thakker, M. Schaefer-Ridder, J.M. Karle, W.W.A.W. Levin, R.L. Chang, A.H. Cohney, Polycyclic Hydrocarbons and Cancer, Academic Press, New York, 1978.
[19] D.L. Poster, M.M. Schantz, L.C. Sander, S.A. Wise, Anal. Bioanal. Chem. 386 (2006) 859.
[20] S. Moret, L.S. Conte, J. Chromatogr. A 882 (2000) 245.
[21] J. de Boer, R.J. Law, J. Chromatogr. A 1000 (2003) 223.
[22] P.M. Kramer, Anal. Chim. Acta 376 (1998) 3.
[23] D. Barcelo, A. Oubina, J.S. Salau, S. Perez, Anal. Chim. Acta 376 (1998) 49.
[24] K.A. Fahnrich, M. Pravda, G.G. Guilbault, Anal. Lett. 35 (2002) 1269.
[25] A. Szekacs, H.M. Le, D. Knopp, R. Niessner, Anal. Chim. Acta 399 (1999) 127.
[26] K. Li, R.L. Chen, B.T. Zhao, M. Liu, A.E. Karu, V.A. Roberts, Q.X. Li, Anal. Chem. 71 (1999) 302.
[27] Y.F. Zhang, Q.M. Zhang, Z.X. Gao, S.G. Dai, J. Agro-Environ. Sci. 25 (2006) 537 (Journal written in Chinese. CAN: 148:162781).
[28] C.R. Spier, E.S. Bromage, T.M. Harris, M.A. Unger, S.L. Kaattari, Anal. Biochem. 387 (2009) 287.
[29] N. Delaunay-Bertoncini, V. Pichon, M.C. Hennion, J. Chromatogr. A 999 (2003) 3.
[30] A.V. Wiznycia, J. Desper, C.J. Levy, Chem. Commun. 37 (2005) 4693.
[31] M.N. Inbasekaran, D.T. Witiak, J. Med. Chem. 23 (1980) 278.
[32] C.J. Wu, F.S. Li, J. Agro-Environ. Sci. 26 (2007) 1080 (Journal written in Chinese. CAN: 150:391462).
[33] G.M. Sheldrick, Acta Crystallogr. A64 (2008) 112.
[34] Y. Li, J.Y. Xia, Li, F.S. Li, Comput. Appl. Chem. 26 (2009) 1503 (Journal written in Chinese. CAN: 152:557814).
[35] D.Y. Wu, Y. Li, F.S. Li, Comput. Appl. Chem. 26 (2009) 329 (Journal written in Chinese. CAN: 151:562151).
[36] M.P. Marco, S. Gee, B.D. Hammock, Trends Anal. Chem. 14 (1995) 341.
[37] C.P. Price, D.J. Newman, Principles and Practice of Immunoassay, Grove's Dictionaries, 1991.
[38] F.S. Li, J.Y. Xia, Y. Li, Agro-Environ. Sci. 27 (2008) 1697 (Journal written in Chinese. CAN: 152:34630).
[39] F.S. Li, F. Sun, X.J. Liu, H.H. Cui, Agric. Sci. China 6 (2007) 964.
[40] M.H. Goodrow, B.D. Hammock, Anal. Chim. Acta 376 (1998) 83.
[41] J. Bernstein, R.E. Davis, L. Shimoni, N.L. Chang, Agnew. Chem. Int. Ed. 34 (1995) 1555.
[42] S.W. Yao, V.H.C. Lopes, F. Fernandez, X. Garcia-Mera, M. Morales, J.E. Rodriguez-Borges, M.N.D.S. Cordeiro, Bioorg. Med. Chem. 11 (2003) 4999.
[43] J.W. Zou, B. Zhang, G.X. Hu, Z.C. Shang, Q.S. Yu, Acta Chim. Sinica 62 (2004) 241 (Journal written in Chinese. CAN: 140:186519).